Chemisorption site of methanethiol on Pt{111}

S. S. Kim, Y. Kim, H. I. Kim, S. H. Lee, T. R. Lee, S. S. Perry, and J. W. Rabalais[a)]
Department of Chemistry, University of Houston, Houston, Texas 77204-5641

(Received 21 May 1998; accepted 26 August 1998)

The chemisorption site of the simplest prototypical model alkanethiol compound, methanethiol $[CH_3SH]$, on a Pt{111} surface in the temperature range 298–1073 K has been investigated by means of time-of-flight scattering and recoiling spectrometry (TOF-SARS) and low-energy electron diffraction (LEED). TOF-SARS spectra of the scattered and recoiled ions plus fast neutrals were collected as a function of crystal azimuthal rotation angle δ and beam incident angle α using 4 keV Ar^+ primary ions. At room temperature, the adsorption of methanethiol produces a partially disordered overlayer that gives rise to a diffuse $(\sqrt{3}\times\sqrt{3})R30°$ LEED pattern and three-fold symmetry in the scattering profiles. Heating this surface layer results in the sequential dehydrogenation of the methanethiol and the formation of S–C species at elevated temperatures. By ~373 K, hydrogen is absent from the TOF-SARS spectra and a sharp $(\sqrt{3}\times\sqrt{3})R30°$ LEED pattern is observed. The model developed from the scattering data is consistent with the preservation of the adsorption site at elevated temperatures, but a change in the S–C bond angle with respect to the surface plane. For the fully dehydrogenated species, the S atoms reside $\sim 1.6\pm 0.2$ Å above the surface in face-centered-cubic (fcc) three-fold sites and the C atoms reside $\sim 1.5\pm 0.4$ Å in hexagonal-close-packed (hcp) three-fold sites. It is proposed that the remarkable stability of this SC adsorbate results from bonding of both the S and C atoms to the surrounding Pt atoms, i.e., a Pt-stabilized SC moiety. © *1998 American Institute of Physics.* [S0021-9606(98)70245-4]

I. INTRODUCTION

Chemisorption of organosulfur compounds such as alkanethiols on metal surfaces forms well-defined organic overlayers known as self-assembled monolayers (SAMs).[1] Synthetic methods for preparing these dense, highly oriented films have been described.[2] A detailed understanding of the structure and molecular packing of these films is essential for understanding their physical properties and chemical reactivity. A variety of experimental analytical techniques[3] along with molecular-dynamics simulations[4] have been employed for characterization of the structure, order, and bonding of SAMs. We have recently[5] applied the technique of time-of-flight scattering and recoiling spectrometry (TOF-SARS) for studying the surface structures of SAMs formed by the adsorption of *n*-alkanethiols $[CH_3(CH_2)_{n-1}SH]$, where $n=16$ and 17, and an alkanethiol with a CF_3 terminal group $[CF_3(CH_2)_{15}SH]$ which were deposited on a Au{111} surface. The highly surface sensitive TOF-SARS technique provides information on the outermost layers of the SAMs. It does not probe down to the sulfur–metal interface which is buried beneath 16 or 17 layers of carbon atoms. In order to probe the nature of the chemisorption site of alkanethiols on the metal surfaces, we have investigated in this study the chemisorption of the simplest prototypical model alkanethiol compound, methanethiol $[CH_3SH]$, on Pt{111} using TOF-SARS. The nature of the chemisorption site of methanethiol on a surface can be determined directly by TOF-SARS since both the adsorbate and the underlying metallic substrate can be probed with the appropriate choice of incident and azimuthal scattering beam angles. Methanethiol is not readily chemisorbed on Au{111} surfaces at room temperature, however, dimethyl disulfide is expected to chemisorb dissociatively to form methylthiolate (CH_3S) on the surface; this system is currently under investigation.[5]

The chemisorption of methanethiol on a variety of different metal surfaces has been studied[6–20] by techniques such as x-ray photoelectron spectroscopy (XPS), temperature programmed desorption (TPD), high-resolution electron energy loss spectroscopy (HREELS), fluorescence yield near edge spectroscopy (FYNES), photoelectron diffraction, scanning tunneling microscopy (STM), and low-energy electron diffraction (LEED). Although this work has generated detailed information regarding the chemisorption of methanethiol on a number of metal surfaces, the exact adsorption site and geometry of this model adsorbate has yet to be determined. In this work, we focus on the chemisorption site of CH_3SH on a Pt{111} surface at room temperature and after annealing to elevated temperatures in an ultrahigh vacuum (UHV) environment. It is pertinent to our study to review the most significant findings from previous works on the CH_3SH/Pt{111} and S/Pt{111} systems.

Previous studies[10,11,18] have shown that CH_3SH adsorbed on Pt{111} at 88 K undergoes sequential dehydrogenation with increasing temperature until all of the hydrogen is desorbed and only sulfur and carbon atoms remain on the surface well above room temperature. These studies have focused on identification of the molecular intermediates on the surface as a function of temperature using the HREELS and XPS techniques. The vibrational modes of methanethiol adsorbed at 88 K match those of the gas-phase infrared (IR)

a)Author to whom correspondence should be addressed. Electronic mail: rabalais@jetson.uh.edu

frequencies of CH_3SH, indicating intact molecular chemisorption. The adsorption species at 158 K is methylthiolate (CH_3S) and hydrogen atoms, as evidenced by the disappearance of the SH bending and stretching modes and the persistence of the characteristic thiolate modes. This thiolate is bound to the surface through the sulfur atom. Heating to 363 K results in further dehydrogenation and formation of adsorbed methylene sulfide (CH_2S). The observation of both Pt–S and Pt–C stretching modes suggests the existence of a bidentate species such as Pt–SCH_2–Pt. At 703 K, only Pt–S and Pt–C modes are observed, indicating complete dehydrogenation. NEXAFS results[18,20] for the chemisorbed species indicate that the S–C bond angle measured from the surface plane is 45° for CH_3S and 20° for CH_2S.

Chemisorption of sulfur atoms on a Pt{111} surface near room temperature produces a $(\sqrt{3}\times\sqrt{3})R30°$ LEED pattern.[21] Quantitative analysis of this LEED data indicates that the sulfur atoms reside in three-fold fcc sites with a Pt–S bond length of 2.28 Å; the bond length of bulk platinum sulfide is 2.32 Å. Ion scattering and LEED studies[22,23] of sulfur atoms on a Ni{111} surface have also suggested that the sulfur atoms reside at three-fold fcc sites with a Ni–S bond length of 2.21 Å; the bond lengths of bulk nickel sulfides are in the range of 2.28–2.38 Å. In general, for sulfur chemisorption on fcc {111} metal surfaces, it is found that the metal-sulfur bond distances are smaller than those occurring in the bulk sulfides.

To the best of our knowledge, the exact position of the chemisorption site of methanethiol has not been determined on the {111}-(1×1) surface of any metal. The objective of this study is to determine the nature of this chemisorption site on the Pt{111} surface. It is generally believed that chemisorption occurs at a three-fold site in which the adsorbate is centered above an equilateral triangle formed by three first-layer atoms.[24] There are, however, two different three-fold sites on {111} surfaces, i.e., the fcc site which is directly above a third-layer atom and the hcp site which is directly above a second-layer atom. The technique of TOF-SARS, coupled with classical ion trajectory simulations, allows a direct real-space investigation of the chemisorption site of CH_3SH at room temperature and elevated temperatures on Pt{111}, the elemental composition of the outermost layers, the surface periodicity, and the behavior of the adsorbate at high temperatures. In addition, TOF-SARS has high sensitivity to surface hydrogen and allows one to probe the involvement of hydrogen in the surface structure.

II. METHODS

The time-of-flight scattering and recoiling spectrometry (TOF-SARS) technique was used for surface elemental analysis and structural characterization. Details of the TOF-SARS technique have been described elsewhere.[25] Briefly, a pulsed noble gas ion beam irradiated the sample surface in a UHV chamber and TOF spectra of the scattered and recoiled ions plus fast neutrals were measured. The primary 4 keV beam employed herein was Ar^+ for scattering from the Pt substrate atoms and for recoiling of H, C, and S atoms. The ion pulse width was ~50 ns, the pulse repetition rate was 30 kHz, the average beam current was 0.5 nA/cm^2, and the TOF drift region was 125 cm long. The total ion dose of $\sim 10^{10}$ ions/cm^2 required for acquisition of a TOF-SARS spectrum produced no observable degradation of the sample surface. The peak intensities were measured as the number of counts above background under the respective peak. The angular notation is defined as follows: α=beam incident angle relative to the surface, δ=crystal azimuthal angle; θ=scattering angel; ϕ=recoiling angle. LEED patterns were obtained with reverse view optics as a function of sample annealing temperature.

The classical shadow cones produced by the repulsive potential of the atomic collisions were calculated by means of the scattering and recoiling imaging code (SARIC) developed in this laboratory. SARIC is based on the binary collision approximation, uses the Ziegler–Biersack–Littmark (ZBL) universal potential to describe the interactions between atoms, and includes both out-of-plane and multiple scattering. Details of the simulation have been published elsewhere.[26,27]

The substrate Pt single crystal with a polished {111} surface was cleaned by repeated cycles of 1 keV Ar^+ sputtering and annealing to 1073 K in the UHV chamber. Annealing was accomplished by electron bombardment heating from behind the crystal. Methanethiol was obtained in 99.5% purity from Matheson Gas Co. Chemisorption of methanethiol was accomplished by exposure to the clean substrate through a leak valve at a pressure of $\sim 2\times 10^{-7}$ Torr for 1 hr. The sticking probability was estimated to be $\sim 1\times 10^{-3}$ by making the assumption that saturation of the CH_3SH spectral features corresponded to chemisorption of a single monolayer.

III. EXPERIMENTAL RESULTS

A. Low-energy electron diffraction pattern

The Pt{111} surface prepared by the procedures previously described exhibited a sharp (1×1) LEED pattern as shown in Fig. 1(a). The incident beam energy for this pattern and each of those shown for the thiol overlayer was 66 eV. Following a saturation exposure to methanethiol at 298 K, a faint $(\sqrt{3}\times\sqrt{3})R30°$ pattern and an increased background intensity were observed in the LEED image in addition to the original (1×1) structure of the Pt surface [Fig. 1(b)]. Heating of this adsorbate layer to 403 K produced a sharpening of the $(\sqrt{3}\times\sqrt{3})R30°$ spots indicative of an ordering of the adsorbate layer [Fig. 1(c)]. Upon heating to 1073 K, the pattern sharpened appreciably; no other diffraction features in addition to the Pt{111}-(1×1) structure were observed [Fig. 1(d)].

B. TOF-SARS spectra

Typical TOF spectra from the clean Pt surface, the surface after exposure to $\sim 7\times 10^2$ L of CH_3SH at 298 K, and the exposed surface after heating to 373 and 1073 K are shown in Fig. 2. The peaks are identified[28] by using the simple binary collision approximation to determine the scattering and recoiling energies and corresponding flight times for the various atomic collisions involved. The clean spec-

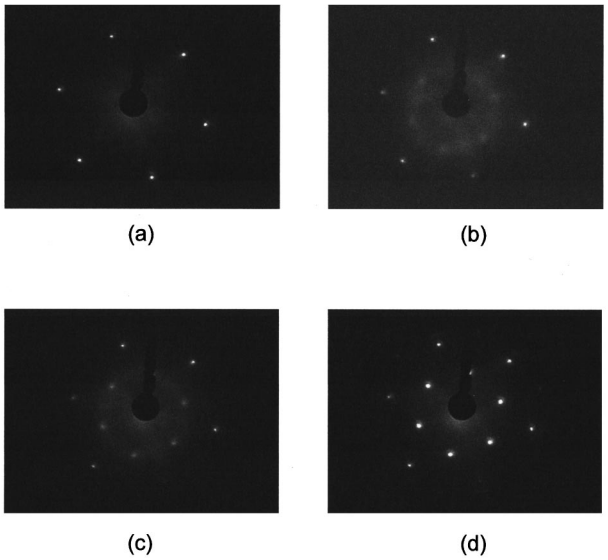

FIG. 1. LEED results for (a) clean Pt{111}, (b) methanethiol chemisorbed on Pt{111} at 298 K, (c) after heating the chemisorbed species to 403 K, and (d) after heating the chemisorbed species to 1073 K.

trum exhibits a sharp, intense peak for Ar scattering from Pt atoms, i.e., Pt(s), which is centered at 11.5 μs. There is no evidence of contaminants in this spectrum. Upon exposure to a saturation dose of CH_3SH, the Pt(s) peak broadens due to multiple scattering contributions and additional peaks appear due to recoil of H, C, and S, i.e., H(r), C(r), and S(r), and Ar scattering from S atoms, i.e., S(s). The S(s) peak is very weak, as expected for scattering of a heavy projectile atom from a light target atom. Heating to the higher temperatures results in loss of the H(r) peak and better definition of the C(r), S(r), and S(s) peaks. The spectra of the adsorbate covered surface at 298 and 373 K exhibit broadened features in the region of the H, C, and S recoils and it is difficult to distinguish the individual peaks in this region. This broadening results from the many degrees of rotational and vibrational freedom of the chemisorbed molecules and the many possible multiple scattering events which produce recoils with broad energy distributions. This is also observed in the increased width of the Pt(s) peak from the exposed surface at 298 K. The H(r) signal is greatly reduced at 373 K, indicating dehydrogenation and desorption of the hydrogen.

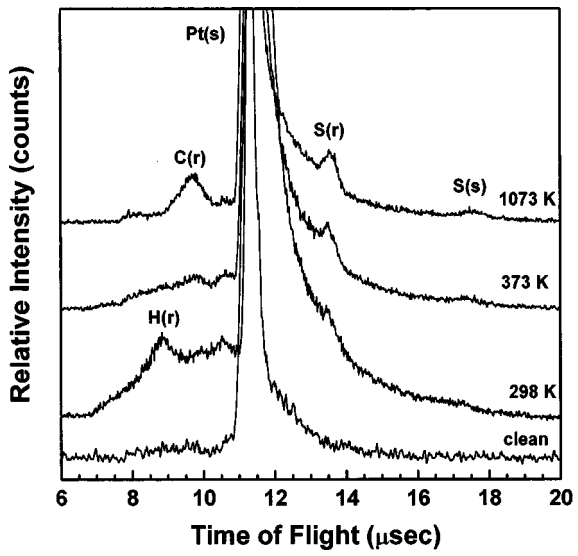

FIG. 2. TOF-SARS spectra of 4 keV Ar^+ scattering and recoiling from a clean Pt{111} surface, the surface after exposure to $\sim 7\times10^2$ L of CH_3SH at 298 K, and after heating the exposed surface to 373 and 1073 K. Incident angle α=23°; Scattering angle β=45°; Azimuthal angle δ=100°.

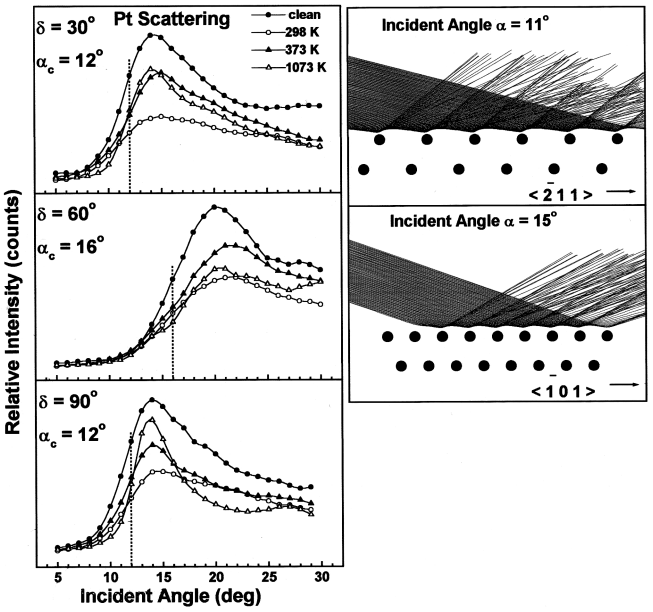

FIG. 3. Incident angle α scans of 4 keV Ar scattering intensity Pt(S) along the three azimuthal directions δ=0°, 30°, and 90° from the clean Pt{111} surface, the surface after exposure to $\sim 7\times10^2$ L of CH_3SH at 298 K, and after heating the exposed surface to 373 and 1073 K. The positions of the critical incident angles α_c are denoted by dashed lines. Ion trajectory simulations are shown on the right side of the scans along planes which are perpendicular to the {111} surface and contain the 0° and 30° azimuths. Bulk interatomic spacings were used for the simulations.

C. Incident angle α scans

Information on the subsurface structure along planes perpendicular to the surface can be obtained[25] by measuring scattering and recoiling intensities as a function of the incident angle α along different azimuthal directions. At grazing α, all atoms lie within the shadow cones of their preceding neighbors. As α is increased, subsurface layer atoms move out of the shadow cones of the first-layer atoms. The impact parameter required for scattering or recoiling into θ corresponds to a critical incident angle α_c where a sharp increase in the scattered or recoiled intensity is observed due to focusing of ions at the edges of the shadowing and blocking cones. The position of α_c provides a direct measure of the first-layer interatomic spacings as shown elsewhere.[25]

1. Ar scattering as a function of temperature

Examples of α scans along three different azimuthal directions are shown in Fig. 3 for Ar scattering from clean Pt and Pt with chemisorbed CH_3SH at 298, 373, and 1073 K. A schematic drawing of the Pt{111} surface along with the azimuthal assignments is shown in Fig. 4. The critical incident angle α_c is measured at the position corresponding to 70% of the peak height. For the clean Pt surface, identical critical

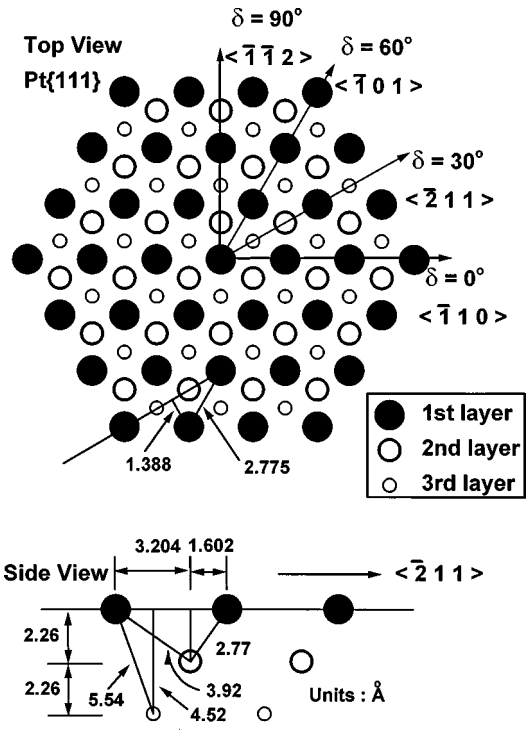

FIG. 4. (upper) Plan view of the ideal bulk-terminated Pt{111} surface illustrating the azimuthal angle δ assignments. (lower) Vertical slice through the surface along the $\langle 211 \rangle$ azimuth showing the ideal interatomic spacings and angles.

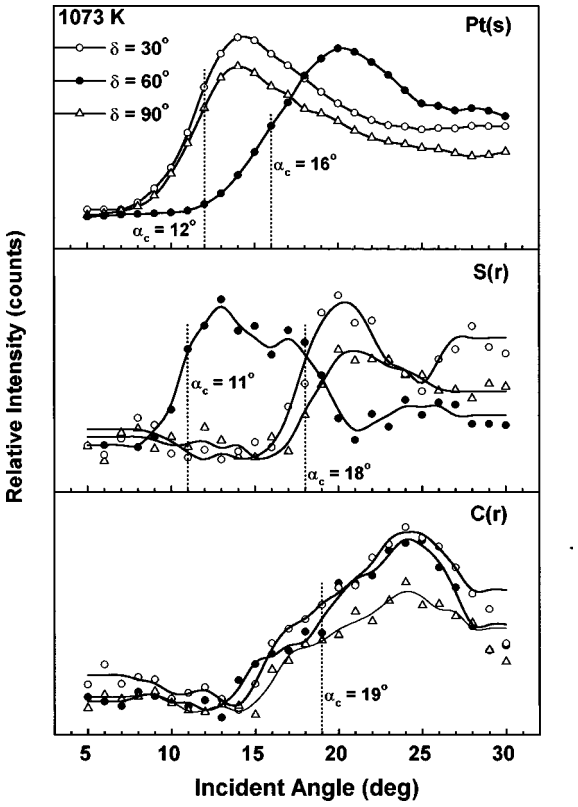

FIG. 5. Incident angle α scans of 4 keV Ar scattering intensity Pt(S) and sulfur and carbon recoiling intensities S(R) and C(R) along the three azimuthal directions δ=0°, 30°, and 90° from the Pt{111} surface after exposure to $\sim 7\times10^2$ L of CH_3SH at 298 K and after heating the exposed surface to 1073 K. The positionis of the critical incident angles α_c are denoted by dashed lines.

angles are observed along the δ=30° and 90° directions at $\alpha_c = 12°$; this value corresponds to a first-layer interatomic spacing of 4.8 Å (as shown in Sec. IV), identifying these directions as either the $\langle 211 \rangle$ or the $\langle 112 \rangle$ crystallographic azimuths. The critical angle observed along the δ=0° direction is $\alpha_c = 16°$; this value corresponds to a first-layer interatomic spacing of 2.8 Å (as shown in Sec. IV), identifying this direction as the $\langle \bar{1}10 \rangle$ crystallographic azimuth. Chemisorption of CH_3SH on this surface results in a lowering and broadening of the intensity profiles of the α scans, although the positions of the α_c's remain constant. This indicates (i) that the chemisorption does not produce any significant change in the Pt first-layer lateral interatomic spacings, i.e., there is no observable relaxation or reconstruction of the Pt{111} structure, and (ii) the S and C atoms provide some attenuation of the Ar trajectories, however, they are inefficient shadowers of the Pt atoms.

Ion trajectory simulations are shown on the right side of Fig. 3 along planes that are perpendicular to the {111} surface and contain the 30° and 60° azimuths. These simulations confirm that the peaks observed in the incident angle scans correspond to scattering from only first-layer atoms and that the critical incident angles α_c result from shadowing of first-layer Pt atoms by their first-layer neighbors. The simulated α_c values, using the bulk interatomic spacings, agree well with the rising slopes of the experimental peaks along both azimuths. This indicates that any change in the first-layer spacings due to relaxation or reconstruction is within the accuracy of the measurement, i.e., the experimental uncertainty is $\pm 2°$, which corresponds to an uncertainty in the interatomic spacing of ± 0.2 Å.

2. Ar scattering and C and S recoiling as a function of temperature

Examples of α scans along the three azimuthal directions identified above for Ar scattering from Pt and C and S recoiling from the chemisorbed surface after heating to 1073 K are shown in Fig. 5. The α_c's for Pt(s) were already discussed in Fig. 3. For S(r), the critical incident angle of the δ=60° scan is $\alpha_c = 11°$ while that of the δ=30° and 90° scans is $\alpha_c = 18°$. These results provide the following clues which will be useful in determination of the ultimate positions of the S atoms: (i) The accessibility of the S atoms to the beam along the δ=30° and 90° azimuths is the same and different from that along the δ=60° azimuth. (ii) The S atoms are severely shadowed or blocked along the 30° and 90° azimuths, i.e., they are only accessible at high α. Along the 60° azimuth, the S atoms are accessible at low α. The α scans for C(r) exhibit a similar behavior for all three δ directions, with a slowly increasing intensity over the broad range of α=15°–25° and centered at $\alpha_c \sim 19°$. This indicates that the C atoms are being shadowed and blocked by more than one neighboring atom and that these neighboring atoms are at different distances from the C atoms.

D. Azimuthal angle δ scans

The surface periodicities of the clean and chemisorbed surfaces were determined[25] by monitoring the scattering and

recoiling intensities as a function of the crystal azimuthal angle δ. TOF spectra similar to those of Fig. 2 were obtained and the intensities of the various peaks were plotted as a function of δ. The minima are coincident with low-index azimuths where the surface atoms are inside of the shadowing and blocking cones cast by their aligned, closely spaced nearest neighbor, resulting in low intensities. As δ is scanned, the atoms move out of the shadow cones along the intermediate δ directions where the interatomic spacings are long, resulting in an increase in intensity. The widths of the minima are related to the interatomic spacings along the particular direction. Wide, deep minima are expected from short interatomic spacings because of the larger degree of rotation about δ required for atoms to emerge from neighboring shadows.

1. Surface periodicity of Pt

Azimuthal angle δ scans of the Ar scattering intensity Pt(s) from the clean Pt{111} surface and the sulfur and carbon recoiling intensities S(r) and C(r) from the surface after exposure to $\sim 7\times 10^2$ L of CH_3SH at 298 K and after heating this exposed surface to 373 and 1073 K are shown in Fig. 6. The δ scan for the clean Pt surface exhibits well-defined 60° periodicity with deep, wide minima along the δ=0°, 60°, and 120° directions due to the short interatomic spacings along these azimuths. The minima along δ=30° and 90° are shallow and narrow due to the long interatomic spacings along these azimuths. Chemisorption of CH_3SH at 298 K results in a drastic reduction of the intensities and lifting of the 60° periodicity. The shapes of the minima at δ=30° and 90° are different after chemisorption, indicating that these two directions are no longer equivalent after chemisorption. This difference becomes more apparent after heating to 373 and 1073 K where three sharp maxima are clearly observed in the region near δ=30°. These three maxima are also present in the 298 K scan, although they are not as sharp and distinct as on the annealed surfaces. This modification of the δ scan of scattered Ar upon chemisorption provides important clues to the nature of the chemisorption site of CH_3SH: (i) The reduction in scattering intensity indicates that the CH_3SH molecule perturbs the scattered ion trajectories, i.e., the molecules reside either on top of or very near the surface. (ii) The lifting of the 60° periodicity shows that the chemisorption pattern reduces the surface periodicity to 120°. (iii) The changes in the scattering features along the δ=30° and 90° directions and the absence of change along the δ=0°, 60°, and 120° directions upon chemisorption indicates that the molecules reside at sites along the δ=30° and 90° azimuths where they can directly perturb scattering trajectories. (iv) The different scattering features along the δ=30° and 90° azimuths indicates that the molecules are chemisorbed in specific sites which are not equivalent when viewed along these two different azimuthal directions.

2. Surface periodicity of S and C

Only minor periodic variations are observed in the δ scans of recoiled S and C upon chemisorption at 298 K. No periodicity was observed in the H recoil scans. These periodic variations increase upon heating to 373 K and become very distinct at 1073 K. The lack of a distinct periodicity at 298 K can be due to at least two phenomena. First, the molecules may not be in well-ordered sites upon chemisorption at room temperature. In this situation, migration of the sulfur moieties on the surface is also possible. Annealing may serve to organize these sulfur moieties into stable, well-ordered sites. Second, the many vibrational and rotational degrees of freedom of a molecule such as CH_3SH on a surface along with the large vibrational amplitudes of such light atoms results in a range of possible target atom positions which tends to obliterate the azimuthal features. The small periodic variations observed at 298 K imply that the molecules are in well-ordered sites, but the periodicities are unclear due to the vibrational and rotational excursions of the atoms. Well defined 120° periodicities are observed for the recoiled S and C upon annealing, particularly for the 1073 K scan.

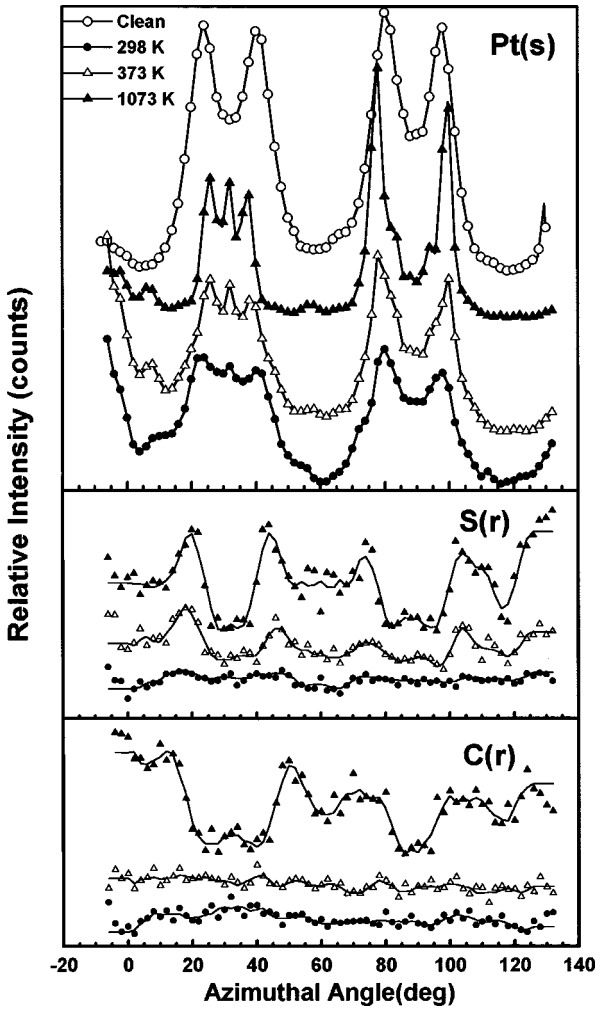

FIG. 6. Azimuthal angle δ scans of Ar scattering intensity Pt(S) and sulfur and carbon recoiling intensities S(R) and C(R) for the clean Pt{111} surface, the surface after exposure to $\sim 7\times 10^2$ L of CH_3SH at 298 K, and after heating the exposed surface to 373 and 1073 K. Incident angle α=13°; Scattering angle θ=45°.

In order to obtain a clearer comparison of the azimuthal differences, δ scans of Ar scattering intensity Pt(s) from the clean Pt{111} surface and the sulfur and carbon recoiling intensities S(r) and C(r) from the surface after exposure to

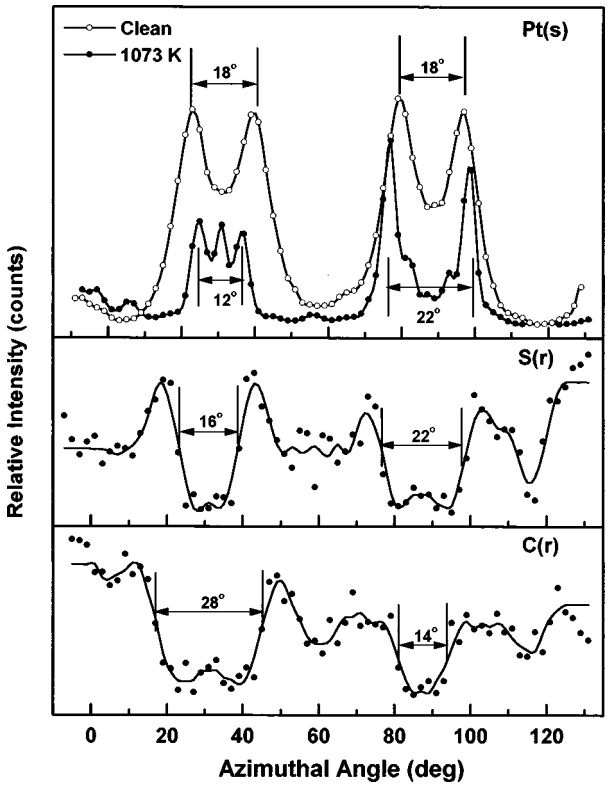

FIG. 7. Azimuthal angle δ scans of Ar scattering intensity Pt(S) and sulfur and carbon recoiling intensities S(R) and C(R) for the clean Pt{111} surface and the surface after exposure to $\sim 7\times 10^2$ L of CH_3SH at 298 K and heating the exposed surfaced to 1073 K. Incident angle $\alpha=13°$; Scattering angle $\theta=45°$.

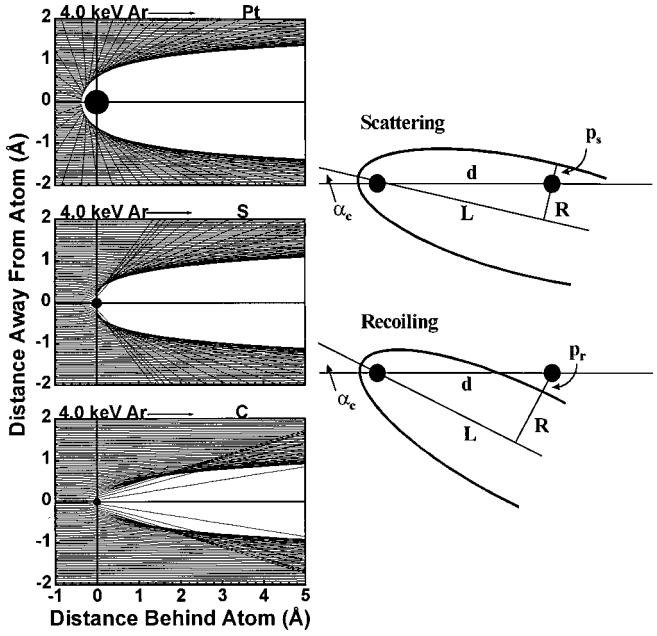

FIG. 8. (Left) Examples of calculated shadow cones for 4 keV Ar collisions with Pt, S, and C atoms. (Right) Schematic diagram showing the use of the experimental critical incident angles (α_c's), the calculated shadow cone shapes, i.e., R vs L, and the calculated impact parameters (p) to determine the positions of the S and C atoms on the Pt surface. The p_s is the impact parameter for scattering of the projectile atom into angle θ and the p_r is the impact parameter for recoiling of a target atom into angle ϕ. R is the radius of the shadow cone at a distance L behind the target atom.

$\sim 7\times 10^2$ L of CH_3SH at 298 K and heating this exposed surface to 1073 K are shown in Fig. 7. The widths of the minima at $\delta=30°$ and 90° are indicated on the figure. These widths are clearly different, in agreement with the observation from Ar scattered off Pt atoms, i.e., the 60° periodicity becomes a 120° periodicity. This can only occur if the adsorbed molecule occupies a distinct three-fold site and the dissociated constituent atoms also occupy distinct three-fold sites. For identification of the specific three-fold site(s) of the adsorbates, it is necessary to resort to the use of classical ion trajectory simulations on models of the chemisorbed surface.

IV. SIMULATION RESULTS

The scattering and recoiling imaging code (SARIC)[26,27] was used for simulation of the shadow cones of Ar scattering from Pt atoms, Ar recoiling of S and C atoms, and the collision impact parameters (p). SARIC is based on the binary collision approximation and allows simulations of interatomic interactions using several different standard potential functions to simulate the three-dimensional motion of atomic particles. Examples of calculated shadow cones for 4 keV Ar collisions with Pt, S, and C atoms are shown in Fig. 8. The accuracy of the Ar/Pt shadow cone shape was verified by using the known Pt interatomic spacings (d's) along specific azimuths and comparison to the experimental critical incident angles (α_c) from Fig. 3. For scattering, the radius R of the shadow cone at a distance L behind a target atom is related to α_c, d, and p_s as

$$R=(d\sin\alpha_c)-p_s \quad \text{and} \quad L=(d\cos\alpha_c), \tag{1}$$

where p_s is the impact parameter for scattering into angle θ. For recoiling, the radius is modified as

$$R=(d\sin\alpha_c)+p_r, \tag{2}$$

where p_r is the impact parameter for recoiling into angle ϕ. These relations are illustrated in Fig. 8. The experimental data of Fig. 3 provided two different experimental values of the (L,R) pair for the two different interatomic spacings along the $\langle 211\rangle$ and $\langle 101\rangle$ azimuths. These experimental values were found to be in excellent agreement with those of the theoretical Ar/Pt cone of Fig. 8. The α_c values obtained from the theoretical cone were within $\pm 1°$ of the experimental α_c values of Fig. 3. The theoretical shadow cones of the Ar→S and C collisions are much smaller than those of the Ar/Pt collisions as shown in Fig. 8. Note that for heavy projectiles colliding with light atoms, some of the scattered trajectories at small p values penetrate into the repulsive potential of the cone, resulting in a poorly defined shadow cone radius. This is particularly apparent for the light C atom. The consequence of this indistinct cone radius and penetration of Ar trajectories is that the C atoms are extremely poor shadowers of neighboring atoms. The S atom provides a somewhat better defined cone radius with little penetration of the Ar trajectories.

V. DETERMINATION OF THE CHEMISORPTION SITE

The chemisorption site of methanethiol and its subsequent dehydrogenation products on Pt{111} has been determined from the LEED pattern, the calculated shadow cones, and the experimental α and δ scans. The data from the 1073 K measurements were used in this analysis since they provided the most distinct features. Since the light H atoms are extremely ineffective shadowing and blocking centers, it is not necessary to include them in the simulations. For example, the maximum deflection angle for an Ar atom scattering from a H atom is $\theta_{max}=\sin^{-1}(M_H/M_{Ar})=1.4°$; this is within the accuracy of the experimental measurements. Therefore, the simulation results obtained for the dehydrogenated SC moiety are equally applicable to the hydrogenated molecule.

There are many possible chemisorption sites and atomic positions that can be selected for the model calculations. The structural information obtained from the LEED data and the incident angle α and azimuthal angle δ scans were used to reduce the number of possible chemisorption sites to a tractable level. The evidence from the experimental data that was used to determine the qualitative site is as follows. (i) The adsorbate periodicity is $(\sqrt{3}\times\sqrt{3})R30°$ (from Fig. 1). (ii) There is no lateral relaxation or reconstruction of the Pt first-layer interatomic spacings upon chemisorption (from Figs. 1 and 3). (iii) The molecules reside either on top of or at the surface (from Fig. 5). (iv) The S atoms are severely shadowed, i.e., they are inaccessible at low α along the 30° $\langle 211\rangle$ and 90° $\langle 11\bar{2}\rangle$ azimuths. This shadowing is dominant along the 90° $\langle 11\bar{2}\rangle$ azimuth (from Fig. 5) as evidenced by the lower peak intensity of this scan. (v) The S atoms are accessible at low α along the 60° $\langle 10\bar{1}\rangle$ azimuth (from Fig. 5), indicating less shadowing along this direction. (vi) The C atoms are shadowed and blocked by more than one neighboring atom and these neighboring atoms are at different distances from the C atoms (from Fig. 5). (vii) The adsorbate molecule resides in distinct three-fold site(s) and the dissociated constituent atoms also occupy similar distinct three-fold sites (from Fig. 6). (viii) These three-fold sites are not equivalent when viewed along the 30° $\langle 211\rangle$ and 90° $\langle 11\bar{2}\rangle$ azimuths (from Fig. 7). (ix) The spectral resolution improves and the features of the α and δ scans become more distinct at higher temperatures (from Figs. 2 and 6).

Using the above evidence and a triangulation approach, the only chemisorption structure that was found to be consistent with all of the experimental data is one in which the S and C atoms are above the surface in fcc and hcp three-fold sites, respectively, as shown in Fig. 9. Alternatively, placing the S and C atoms in hcp and fcc sites, respectively, results in poor agreement with the incident angle scans of Fig. 5. Since the chemisorption sites are above the surface and the S and C atoms are poor shadowers of Pt atoms, it was not possible to obtain a direct experimental determination of the heights of the S and C atoms above the Pt surface. In order to probe the viability of the proposed structure, the position of the S atom was fixed above the fcc site at a distance of 2.2–2.4 Å, corresponding to the known range of Pt–S bond lengths. Using such a model and the calculated shadow cones of Fig. 8, it is shown in Fig. 9(a) that the S atoms are shadowed by their neighboring S atoms in adjacent fcc sites. They are too high above the Pt surface to be shadowed by Pt atoms at the α_c values of Fig. 5. Using this fixed range of heights for the S atoms, the C atoms were placed above the hcp sites. The α_c values of Fig. 5 for the C atoms range from 15° to 25°, consistent with C atoms being shadowed by neighboring S atoms at adjacent fcc sites, neighboring C atoms at adjacent hcp sites, and other neighboring atoms as shown in Fig. 9(b). These data are consistent with the S and C atoms residing at sites that are $\sim 1.6\pm 0.2$ and $\sim 1.5\pm 0.4$ Å, respectively, above the surface and Pt–S, Pt–C, and S–C bond distances of $\sim 2.3\pm 0.1$, 1.7 ± 0.1, and 2.2 ± 0.2 Å, respectively, as shown in Fig. 9(c). The S–C moieties are shown in Fig. 9(d) arranged in a $(\sqrt{3}\times\sqrt{3})R30°$ pattern with the S atoms in fcc sites and the C atoms in hcp sites aligned along the $\langle 211\rangle$ azimuth at $\delta=30°$. These C atoms could also occupy the equivalent hcp sites aligned with the $\langle 11\bar{2}\rangle$ azimuth at $\delta=90°$ or the $\langle 211\rangle$ azimuth at $\delta=-30°$. Random occupancy of these equivalent hcp sites by the C atoms would still give a $(\sqrt{3}\times\sqrt{3})R30°$ pattern.

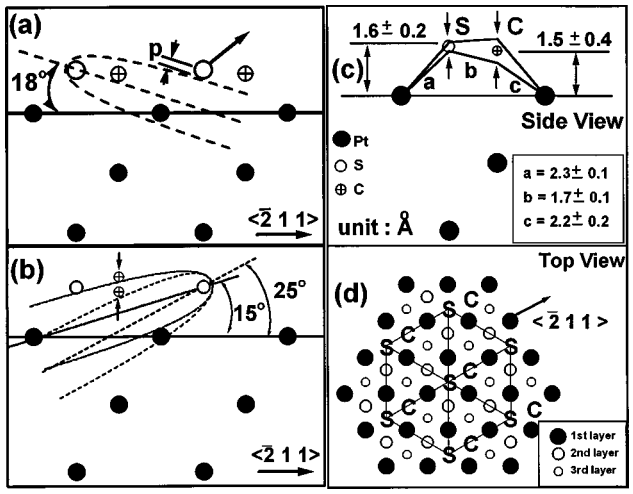

FIG. 9. Illustration of the use of experimental critical incident angles α_c and the calculated shadow cones to determine the interatomic spacings and relative heights of (a) the S atoms and (b) the C atoms on the Pt{111} surface. (c) Final positions of the S and C atoms above the Pt{111} surface as determined from the TOF-SARS and LEED results. (d) Illustration of an S–C adsorbate structure that would produce a $\sqrt{3}\times\sqrt{3})R30°$ LEED pattern.

The above analysis is based on the elevated temperature data. The room temperature data are qualitatively similar. The 298 K LEED pattern has the same symmetry $[(\sqrt{3}\times\sqrt{3})R30°]$ as the 993 K pattern, although it is faint and has an increased background intensity; the original (1×1) structure of the Pt surface remains (Fig. 1). The 298 K TOF-SARS incident and azimuthal angle scans have the same features as the 1073 K data, although they are broadened and less distinct (Figs. 3 and 6). These results indicate that the room-temperature chemisorption site is similar to that at the higher temperatures, although the heights of the S and C atoms above the surface may be different and the adsorbates may not be as well ordered as they are at higher temperatures.

VI. DISCUSSION

This TOF-SARS and LEED study of the evolution of the CH_3SH molecule on a Pt{111} surface as a function of temperature has enabled a characterization of the chemisorption site of the molecule. The experimental data combined with the simulation results clearly indicate that chemisorption at 298 K occurs at a specific three-fold site and that this site is qualitatively unchanged upon annealing to high temperatures. The observed perturbation of the Ar scattering from Pt azimuthal features upon chemisorption result from the S and C atoms on the surface, rather than the light H atoms. The presence of the H atoms serves only to broaden the spectral and azimuthal features. This is evidenced by the sharpening of these features as a function of temperature commensurate with the observation of the desorption of hydrogen, which is essentially complete at temperatures just above 373 K. The absence of azimuthal anisotropy in the H atom δ scans implies that the methyl groups have free rotation about the S–C bond of the chemisorbed molecule, i.e., the H atoms are not localized at distinct sites on the surface where they could be selectively shadowed and blocked by S and C atoms. The dehydrogenation ultimately results in a weakening of the S–C bond. Taken together, these results indicate that the chemisorption sites of the S and C atoms in chemisorbed methanethiol at 298 K are similar to their positions after annealing to 1073 K, where there is complete dehydrogenation.

The results show that the S and C atoms are anchored at the fcc and hcp sites, respectively, even at 1073 K, so that the S–C interatomic distance at this high temperature is equivalent to the interatomic distance at low temperature. The work of Rufael, *et al.* is, especially pertinent to this implication. Using HREELS, TPD, NEXAFS, and XPS, Rufael, *et al.*[10,11] found that the low-temperature chemisorbed species is methylthiolate (CH_3S) and that sequential dehydrogenation occurs as a function of increasing temperature, producing CH_nS surface species, where n=1, 2, and 3. The highest temperature for which hydrogen stretching frequencies were still observed in the molecule was in the range of 363–378 K. Since both Pt–S and Pt–C stretching modes were also observed at this temperature, it was suggested that a bidentate species such as Pt–SCH_2–Pt existed on the surface. The data indicated an inclination of the S–C bond angle of 45° and 20° from the surface plane for CH_3S and CH_2S, respectively, with the sulfur end of the moiety nearest to the surface. Rufael *et al.*,[10,11] did not determine the nature of the chemisorption site(s) from their data.

Based on our experimental data and simulations, we propose that chemisorption of CH_3SH in UHV at 298 K produces CH_3S species that then undergo sequential dehydrogenation. The resulting CH_nS species are bonded to the surface through both the S and C atoms at the three-fold sites specified above. Thermally induced sequential dehydrogenation occurs. The S–C bond angle with the surface is largest for the methylthiolate species, where the molecule is bonded through the S atom. As dehydrogenation progresses, the bond angle with the surface decreases and the molecule assumes well-ordered three-fold sites. For the fully dehydrogenated species, the S atoms reside $\sim 1.6 \pm 0.2$ Å above the surface in fcc three-fold sites and the C atoms reside $\sim 1.5 \pm 0.4$ Å in hcp three-fold sites. This indicates that the Pt–SCH_2–Pt complex is dehydrogenated to a Pt–S–C–Pt complex at high temperature and that this complex remains intact even at 1073 K. The remarkable stability of this species must result from bonding of both the S and C atoms to the surrounding Pt atoms, i.e., a Pt-stabilized SC moiety.

Our results have direct implications for the self assembly of long chain alkanethiols on metal surfaces. First, our observation that methanethiol bonds through the S atom at fcc three-fold sites on Pt(111) suggests that alkanethiols might bind with similar site selectivity on other noble metals such as silver, gold, and copper. Determining the exact mode of bonding of long chain alkanethiols on surfaces is likely to permit a more detailed rationalization of the observed stabilities and reactivities of SAMs. Second, our observation that both the S and C atoms are bound to the surface at elevated temperatures in the form of a Pt–SC–Pt moiety is surprising in light of the proposal that SAMs on Au{111} decompose via cleavage of the sulfur–carbon bond.[29] One might expect that adsorption on platinum, which is highly active in catalyzing several types of bond-cleaving reactions (including S–C bonds in hydrodesulfurization[30]), would more readily lead to S–C cleavage than adsorption on gold, which is relatively inert catalytically. The stability of the Pt–SC–Pt moiety likely arises from the strength of the S and C atom bonds to the Pt three-fold sites. These results suggest that decomposition of SAMs on Pt{111} may occur by C–C bond cleavage rather than C–S bond cleavage at elevated temperatures.

VII. CONCLUSIONS

The results of TOF-SARS and LEED measurements show that methanethiol is chemisorbed at 298 K on a Pt{111} surface in a $(\sqrt{3}\times\sqrt{3})R30°$ structure with a sticking probability of $\sim 1\times 10^{-3}$. Sequential dehydrogenation occurs as the temperature is increased. Structural analysis indicates that the S atoms reside above the fcc three-fold sites and the C atoms reside above the hcp three-fold sites, with the S–C bond angle decreasing as H atoms are loss from the methyl group. At elevated temperatures the S–C bond is approximately parallel to the surface. The observation of this structure at temperatures as high as 1073 K suggests a remarkable stability for a Pt-stabilized SC moiety. These findings suggest that the fcc three-fold site is the most stable position for bonding of thiol based self-assembled monolayers to a Pt{111} surface.

ACKNOWLEDGMENTS

This material is based in part on work supported by the National Science Foundation under Grant No. CHE-9700665, the R. A. Welch Foundation under Grant No. E656, and the Texas Advanced Research Program under Grant No. 3652-683.

[1] For a recent review, see: A. Ulman, Chem. Rev. **96**, 1533 (1996).
[2] G. M. Whitesides and P. E. Laibinis, Langmuir **6**, 87 (1990).
[3] Edited by A. Ulman, *Characterization of Organic Thin Films* (Butterworth-Heinemann, Boston, Massachusetts, 1995).
[4] R. Bhatia and B. J. Garrison, Langmuir **13**, 4038 (1997); H. Morgner, *ibid.*

13, 3990 (1997); W. Mar and M. L. Klein, *ibid.* **10**, 188 (1994).
[5] L. Houssiau, S. S. Perry, T. R. Lee, and J. W. Rabalais (work in progress).
[6] D. R. Mullins, T. Tang, X. Chen, V. Shneerson, D. K. Saldin, and W. T. Tysoe, Surf. Sci. **372**, 193 (1997).
[7] M. H. Dishner, J. C. Hemminger, and F. J. Feher, Langmuir **13**, 2319 (1997).
[8] T. S. Rufael, D. R. Huntley, D. R. Mullins, and J. L. Gland, J. Phys. Chem. **99**, 11472 (1995).
[9] D. R. Mullins and P. F. Lyman, J. Phys. Chem. **99**, 5548 (1995); **97**, 12008 (1993); **97**, 9226 (1993).
[10] T. S. Rufael, R. J. Koestner, E. B. Kollin, M. Salmeron, and J. L. Gland, Surf. Sci. **297**, 272 (1993).
[11] T. S. Rufael, J. Prasad, D. A. Fischer, and J. L. Gland, Surf. Sci. **278**, 41 (1992).
[12] B. C. Wiegand, P. Uvdal, and C. M. Friend, Surf. Sci. **279**, 105 (1992).
[13] M. E. Castro and J. M. White, Surf. Sci. **257**, 22 (1991).
[14] M. E. Castro, S. Ahkter, A. Golchet, J. M. White, and T. Sahin, Langmuir **7**, 126 (1991).
[15] M. R. Albert, J. P. Lu, S. L. Bernasek, D. D. Cameron, and J. L. Gland, Surf. Sci. **206**, 348 (1988).
[16] D. R. Huntley, J. Phys. Chem. **93**, 6156 (1988).
[17] R. G. Nuzzo, B. R. Zegarski, and L. H. Dubois, J. Am. Chem. Soc. **109**, 733 (1987).
[18] R. J. Koestner, J. Stohr, J. L. Gland, E. B. Kollin, and F. Sette, Chem. Phys. Lett. **120**, 285 (1985).
[19] J. B. Benziger and R. E. Preston, J. Phys. Chem. **89**, 5002 (1985).
[20] J. Stohr and R. Jaeger, Phys. Rev. B **26**, 4111 (1982).
[21] K. Hayek, H. Glassl, A. Gutmann, H. Leonhard, M. Prutton, S. P. Tear, and M. R. Welton-Cook, Surf. Sci. **152/153**, 419 (1985).
[22] Y.-S. Ku and S. H. Overbury, Surf. Sci. **276**, 262 (1992).
[23] D. R. Mullins, D. R. Hyntley, and S. H. Overbury, Surf. Sci. **323**, L287 (1995).
[24] For an excellent description of studies of SAMs on gold, see: N. Camillone III, C. E. D. Chidsey, G.-y Liu, and G. Scoles, J. Chem. Phys. **98**, 4234 (1993).
[25] J. W. Rabalais, Science **250**, 521 (1990); O. Grizzi, M. Shi, H. Bu, and J. W. Rabalais, Rev. Sci. Instrum. **61**, 740 (1990).
[26] V. Bykov, C. Kim, M. M. Sung, K. J. Boyd, S. S. Todorov, and J. W. Rabalais, Nucl. Instrum. Methods Phys. Res. B **114**, 371 (1996).
[27] M. M. Sung, V. Bykov, A. Al-Bayati, C. Kim, S. S. Todorov, and J. W. Rabalais, Scanning Microsc. **9**, 321 (1995).
[28] J. W. Rabalais, CRC Crit. Rev. Solid State Mater. Sci. **14**, 319 (1988).
[29] C.-J. Zhong and M. D. Porter, J. Am. Chem. Soc. **116**, 11616 (1994).
[30] For a recent example, see M. Sugioka, L. Andalaluna, S. Morishita, and T. Kurosaka, Catal. Today **39**, 61 (1997).